UHV-HREM and Diffraction of Surfaces

G. JAYARAM, R. PLASS AND L.D. MARKS
Department of Materials Science and Engineering, 2036 MLSF, 2225 N. Campus Drive, Northwestern University, Evanston, Il 60208

Abstract. Characterization of the structure of surfaces is very important in order to develop a fundamental understanding of the electronic, mechanical and chemical properties of a material. While transmission electron microscopy imaging (TEM) and diffraction (TED) techniques are capable of providing surface structural information at the atomic level, such data would be suspect if obtained under conventional vacuum conditions (10^{-6}–10^{-8} Torr). Ultrahigh vacuum (UHV) conditions are imperative during both preparation and observation of clean surfaces/interfaces. Conventional TEM techniques are very powerful for UHV-TEM investigations; however, the marriage of surface science and conventional TEM to yield an UHV-TEM is a complex task. These complexities and some of the results obtained using UHV-TEM and UHV-TED techniques for surfaces i.e. solid-vacuum interfaces will be illustrated.

Keywords: ultrahigh vacuum (UHV), transmission electron microscopy (TEM) imaging, electron diffraction, surfaces

Introduction

It has long been known that the surface of a material possesses properties totally different from the bulk; this arises from the difference in local coordination of the atoms at the surface and consequently gives rise to different electronic, chemical and mechanical properties in comparison to the bulk. The local coordination is strongly influenced by numerous mechanisms operating at the surface. These include condensation and adsorption of gas phase molecules from the surrounding environment which can nucleate clusters or diffuse either on or into the surface; evaporation of the surface or adsorbate atoms into the ambient is also possible (see [1]). While for a surface in thermodynamic equilibrium with the environment, these processes would all proceed in opposite directions with equal rates, most real life processes like thin film growth are non-equilibrium kinetic processes; the final morphology depends on the balance between these processes. The surface can be thought of as representing an *interface* between the solid and the surrounding environment; the characterization of this interface, both chemically and structurally, is the building block for understanding the behavior of solid-solid interfaces e.g. thin film growth on solid surfaces which are of high relevance in many technological applications. The properties of these systems are strongly controlled by

the initial stages of nucleation and growth during epitaxy which in turn are influenced by the competitive processes described above (for excellent reviews on the basic mechanisms operating in the early stages of thin film epitaxial growth see [1–2]). Characterization of surface properties needs to be performed under a highly controlled UHV environment to be meaningful. Once a fundamental understanding of the atomistic processes is obtained under UHV conditions, extrapolation to the more complex real-life behavior becomes simpler.

Surface Characterization Techniques

Surface characterization studies are conventionally carried out in two modes: *in situ* where the individual kinetic processes are imaged in real time and *ex situ* where assumptions have to be made to deduce the actual operating mechanism. Although *in situ* real time measurements are highly desirable, they place strict constraints on design and the type of experiments possible; trade-offs between resolution, speed of measurement and information content become unavoidable. Both modes of studies mainly use an incident electron or photon beam and analyze the exiting electrons or photons. Techniques that use incident electrons and image using exiting electrons include scanning electron microscopy (SEM), scanning transmission electron

microscopy (STEM), scanning tunneling microscopy (STM), transmission electron microscopy (TEM), reflection electron microscopy (REM) and low energy electron microscopy (LEEM). Information about the reciprocal space geometry i.e. diffraction, is also available using companion diffraction techniques such as low energy electron diffraction (LEED), reflection high energy electron diffraction (RHEED) and transmission electron diffraction (TED) while chemical characterization is possible using Auger electron spectroscopy (AES). Incident photon based techniques for surface studies include x-ray photoelectron spectroscopy (XPS), ultraviolet photoemission spectroscopy (UPS), photoelectron emission microscopy (PEEM) and x-ray diffraction (XRD).

The electron imaging and diffraction techniques mentioned above differ (from each other) on the basis of the energy and geometry of the beam incident on the specimen, and provide surface information at different sensitivities i.e. resolution and imaging speed. Transmission techniques also differ in one quite fundamental way from all of the others, namely the surface sensitivity of the scattering process. All the other techniques use processes which are specifically surface sensitive, i.e. the majority of the signal comes from the first few surface monolayers; in contrast, the surface signal in transmission is relatively weak but still strong enough to be separated from that of the bulk. It is impossible to adequately describe all of these techniques in detail within the scope of this paper and the interested reader is referred to some excellent review articles on SEM [3–4], STEM [5], REM [6] and XRD [8–9]. However, in the context of reviewing the use of TEM and TED in looking at surfaces and interfaces, it is appropriate to contrast some of the other electron based (incident or exiting) techniques.

Relatively low resolution, high speed imaging is possible using REM, LEEM and PEEM. Of these three microscopies, REM is the best established and has been used in real time to study growth, electromigration and surface structural changes induced on heating to temperatures as high as 1200°C [10–13]. However, geometric distortions are introduced by the grazing incidence and the resolution is limited (at present) to about 0.9 nm perpendicular to the beam. The diffraction mode RHEED can also provide information on the surface structure and/or morphology during thin film deposition in both the static and dynamic modes; an example for the latter being the real time dynamic surface measurements performed during MBE growth of GaAs(001) [14–16]. Distortion of the image is avoided

by LEEM (which uses normally incident electrons) and PEEM (incident photons). Very low energy electrons ($\sim$5–200 eV) are used in LEEM and LEED studies to achieve high surface sensitivities. LEEM has been used to image thermally activated surface processes [17–18], including changes in surface morphology [19] and to image, in real time, epitaxial growth during metal deposition [20–24] with a spatial resolution of, currently, 20 nm. Intensities in LEED patterns have been quantified and used to identify and resolve many surface structures e.g. the simple dimer structure of the Si(100)-2 $\times$ 1 surface was first proposed [25] and subsequently modified using LEED [26]. Spectroscopic variations of LEEM can also be used to provide spatially resolved compositional information (Auger electron emission spectroscopy), albeit with corresponding loss of speed [27–28]. In comparison to REM and LEEM, PEEM has a lower resolution (of about 200 nm) due to the energy spread of the incident photons when no energy analyzer is used; this has however proved to be more than adequate in resolving the spatial chemical kinetics of reaction processes [29]. Addition of an energy analyzer improves the spatial resolution (down to 10–50 nm) at the cost of speed [30–35].

In the above cases, imaging is done in the parallel mode of operation; signals can also be collected in the serial mode using scanning techniques like the SEM, STEM and STM. SEM scans the incident electron beam over the surface and uses the secondary electrons from the sample. Resolution down to 5–10 nm can be obtained using a field emission cathode [36] and when used under UHV conditions can have submonolayer sensitivity [37–39]. In STEM, an electron probe is scanned serially over the sample, similar to a SEM, and the transmitted electrons as well as any surface scattering processes used to obtain images [40–43]. With this approach, Auger images at a resolution of about 2 nm have been obtained. In principle, the type of imaging techniques used to image surfaces in transmission (see below) can also be used in such an instrument, although to date this has not been done. In many respects rather similar to these two, STM uses an atomically sharp metal tip to scan at heights $\sim$0.5 nm above the surface; the tunneling current between the tip and the surface is used to probe the local structure and morphology. Lateral and vertical resolutions down to 0.3 nm and 0.001 nm are obtainable using STM; however there is a smaller field of view, the data collection is slower and is limited by the scanning speed of the tip. In addition to surface structure information on the atomic level, it is also possible to image real time

kinetic processes e.g. formation of domains [44], motion of steps [45], vacancies [46] and static processes e.g. epitaxial growth [47–48] using a STM.

The limitations of the most of the techniques described above (excepting STEM and STM) are that the probe averages over a large area and thus information from near-ideal crystal regions, regions with imperfections like steps, kinks etc. all contribute to the final signal. An inherent limitation therefore is that inhomogeneous surface processes at the atomic level, which play a significant role in case of thin film epitaxy, cannot be characterized. STM studies are limited to conducting materials since electrons have to tunnel between the tip and the surface. Also, while the techniques of LEEM, REM and STM can provide information on the surface layers, they do not provide any information on the interaction of the bulk defects with the surface. Erroneous interpretation of the state of the material is possible when one looks at just the LEED and RHEED patterns e.g. sharp reconstruction spots in LEED and RHEED patterns are usually taken as indicators of a well ordered material; however, a TEM image from a region showing similar patterns in case of Si(111)-7 × 7 [49] reveals an extensive amount of defects in the bulk as illustrated in Fig. 1. Although the very high surface-only sensitivity of the STM provides an excellent picture of the surface structure, it has also proved to be a limitation in other cases e.g. in deciphering the structure of the reconstructed Si(111)-7 × 7 surface where the reconstruction process proceeds many layers into the bulk. In this regard therefore, a technique that is highly sensitive to both the surface and the bulk and that can also be interfaced with chemical characterization techniques is highly desirable.

Transmission electron microscopy and the companion transmission diffraction (TED) techniques offer such a solution. In contrast to the STM, TEM can look at both the surface and the bulk at the same time, and has similar atomic resolution e.g. of Bi atoms on Si(111) surface [50] and the Ir(001)-5 × 1 surface [51]. TEM also provides information on the subsurface defects and can look at rough surfaces and insulators. Dynamic processes like surface modifications under high temperatures and gas etching treatments [52] and *in situ* growth [53–54] can also be imaged. In combination with *in situ* chemical analysis, TEM can be used as a powerful analytical tool. Since in the plan view transmission geometry, as described below, the electrons carry information from both the surfaces (top and bottom) and the bulk, isolating surface information is a more complex task. Also, unlike STM, SEM, REM

etc. which can look at bulk crystals, extensive sample preparation is required so that the crystal is electron transparent i.e. a few hundred Angstroms thick ideally.

Imaging Modes in Transmission

Information about the atomic arrangement at the surface is usually obtained by a combination of imaging and diffraction techniques in TEM studies. Based solely on the orientation of the imaged surface to the incident beam, (for some general reviews, refer to [55–58]) techniques can be broadly classified into two: plan view imaging, in which the top and bottom surfaces are imaged, and profile imaging, where the side surface i.e profile is imaged.

a) **Profile Imaging:** In this case, the electron beam is parallel to the surface of interest. The surface involved is very thin and under the correct defocus conditions [59], the image can be interpreted in terms of the atomic positions on the surface. This mode provides information about displacements/relaxations along the side surface i.e. normal to the top and bottom surfaces and also translations perpendicular to the beam. It was first used to study the Au(110)-2 × 1 surface [60] and small particles [61] and has been used with considerable success in imaging surfaces of gold [60, 62], silicon [63], germanium [64] and cadmium telluride [65]. Although very powerful, it suffers from two problems: One of these is due to the fact that the surface imaged is very thin, and the structures may not accurately represent extensive two-dimensional surfaces. A more fundamental limitation is that a very thin region of surface is intrinsically thermodynamically unstable, so obtaining an equilibrium surface configuration is exceedingly difficult if not impossible.

b) **Plan View Imaging:** In this case, the electron beam is normal to the surface of interest and interacts with the top and bottom surfaces and the bulk material in between. A very important advantage is that one can approach thermodynamically stable flat surfaces, unlike the profile mode. One might think that the surface information would be obscured by the far stronger bulk scattering processes, but this is not the case and it has turned out to be surprisingly simple to obtain surface information. As a consequence of this, all the standard electron microscopy imaging techniques (e.g. bright field, dark field and high resolution) can be used. While conventional high
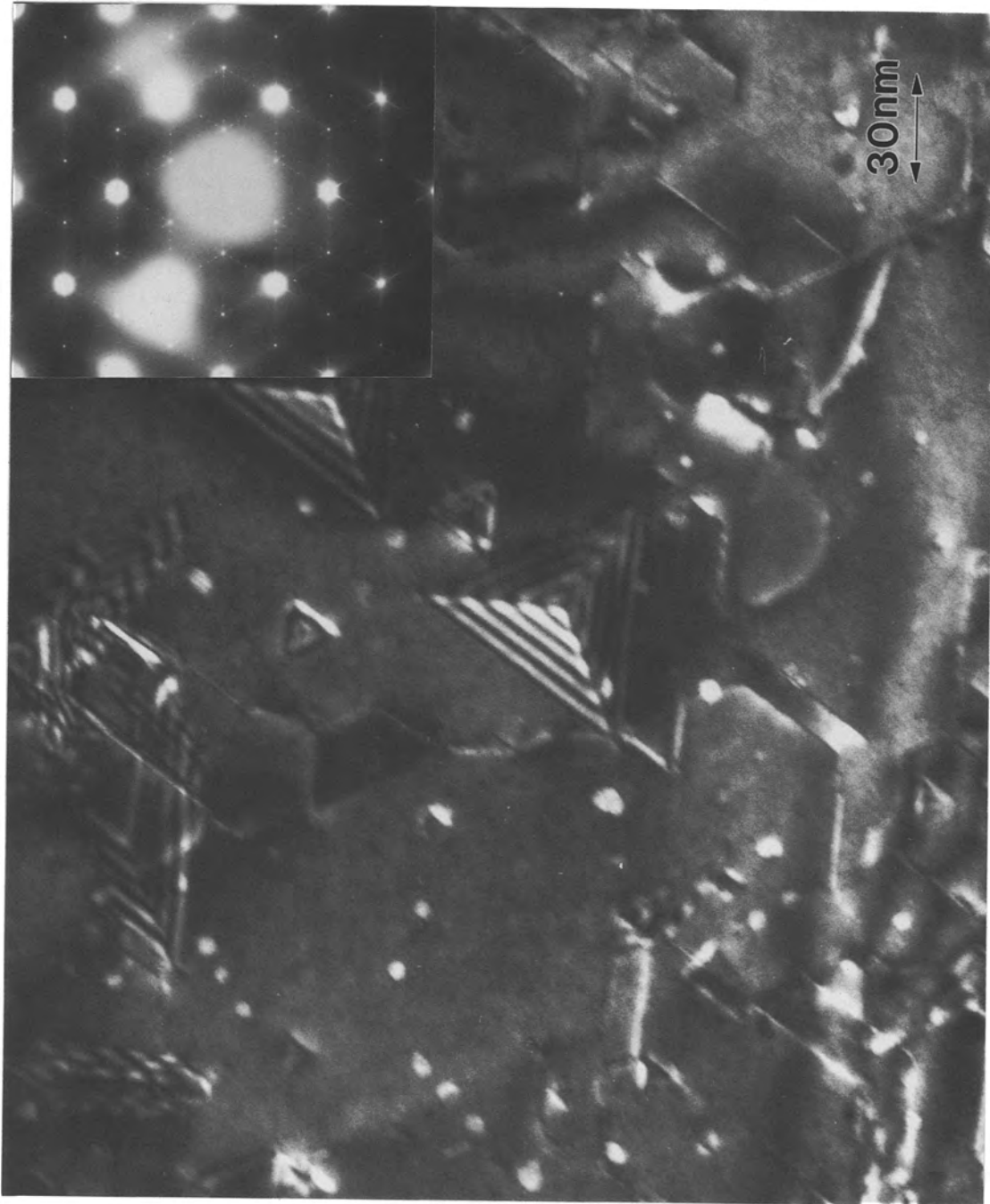
Fig. 1. Dark field image of a Si(111) specimen taken from a region showing the sharp reconstruction spots in the inset diffraction pattern clearly demonstrates the co-existence of numerous stacking faults and stacking fault tetrahedra alongwith the reconstruction.

resolution TEM uses the transmitted beam and all the exiting diffracted beams, the bright field mode uses only the transmitted beam while the dark field mode uses specific diffracted beams for imaging purposes. In the low resolution mode, the latter two techniques are used in defect and strain field analyses. In a higher resolution mode, these can provide information on the surface domains ([66–68]); surface steps have been imaged using the bright field mode e.g. MgO [68] while dark field imaging using forbidden reflections can be used to obtain contrast from surface terraces with atomic height steps as in case of Au(111) [69] and Au(001) [70]. Atomic scale steps on thin MgO crystals have also been revealed using weak-beam dark field imaging [71].

Conventional high resolution plan view imaging can be performed in either the zone axis mode where the incident electron beam is parallel to a major zone axis of the material or in the off-zone axis mode i.e. tilting off a zone axis. High surface sensitivities can be obtained in the latter case as was demonstrated for the Si(111)-7 × 7 surface by [72–73]. This technique is also very powerful at monitoring *in situ* thin film growth on clean surfaces e.g. Au/GaAs(110) [74] and Au, Cu and Pd on clean surfaces of Si(111) [75–76]. The structure of such buried interfaces can also be revealed by using this mode in combination with the cross-sectional TEM mode (involves post-deposition sample preparation to look at interfaces in cross-section) as in case of Ag/Si(100) and Ag/Si(111) interfaces [77]. A schematic of these two modes of imaging is shown in Fig. 2.

Aside from the imaging modes described above, information on the surface atomic positions can be obtained by exclusively using the intensities of the surface diffraction spots in numerical calculations. Although the diffraction and imaging techniques as illustrated above are each capable of providing information on the atomic scale of the surface, some combination of these techniques is almost always used to resolve the structure.

Instrumentation

While investigations of surfaces at the atomic scale using conventional microscopes (vacuum of 10^{-6} to 10^{-8} Torr) are now fairly commonplace, study of *clean* surfaces necessitates a well-controlled UHV environment. Further, *in situ* thin film growth and/or annealing

studies require incorporation of the accessories on the column itself which might affect the resolution; a compromise is an attached UHV-surface science chamber. In both cases, there exists the problem of damping out the vibration induced by the add-ons; a challenge is therefore involved in designing a functional UHV-TEM and their sparse number bear strong testament to this fact (for a review of developments in UHV-TEM technology see [78]).

The possibility of using a TEM to study *in situ* growth was first explored inside an unmodified commercial TEM in 1950 by McLauchlan et al. [79] and later by Bassett [80]; the latter investigation demonstrated the need for better vacuum conditions around the specimen. An earlier study by Ennos [81] had also established that in conventional vacuum (~1 mPa) TEM's, carbonaceous contamination would result from electron bombardment of the residual hydrocarbons. While these studies suggested the need for controlled UHV conditions around the sample region, it was only in the late 1960's that rapid advances in stainless steel UHV technology enabled the first UHV-TEM's to be fabricated.

Initial approaches to attain UHV conditions at the specimen region used either cryopumps [82–84] or an independent UHV chamber around the sample [85–86]. In an effort to improve the vacuum conditions at the specimen region however, in certain cases, specimen exchange and tilting facilities were compromised (for other reviews on UHV-TEM design for *in situ* studies, see [87–88]). On the other hand, the addition of the accessories i.e. for ion sputtering, annealing, gas etching, thin film deposition, RHEED etc. onto the TEM column itself would sometimes compromise the final pressure to the 10^{-9} Torr range due to degassing from viton seals, components etc. [89–90]. In other cases, where such add-ons necessitate considerable volume changes in the pole piece region of the TEM, compromise on the HREM capabilities are inevitable [91]. However, moderate resolution [87, 92] and in other cases, high resolution [93] studies have been reported by some groups using the *in situ* design approach. The latest *in situ* UHV-TEM designs reveal the two different current pumping technology approaches. Similar to the earliest *in situ* UHV-TEM design approaches, a cryopump is used in [93] to attain UHV conditions at the specimen. Cryofingers are in general disadvantageous since they are both bulky and induce vibration, thus in most cases, the resolution is compromised; the attractive alternative option is to use some combination of turbomolecular pumps, ion pumps and titanium
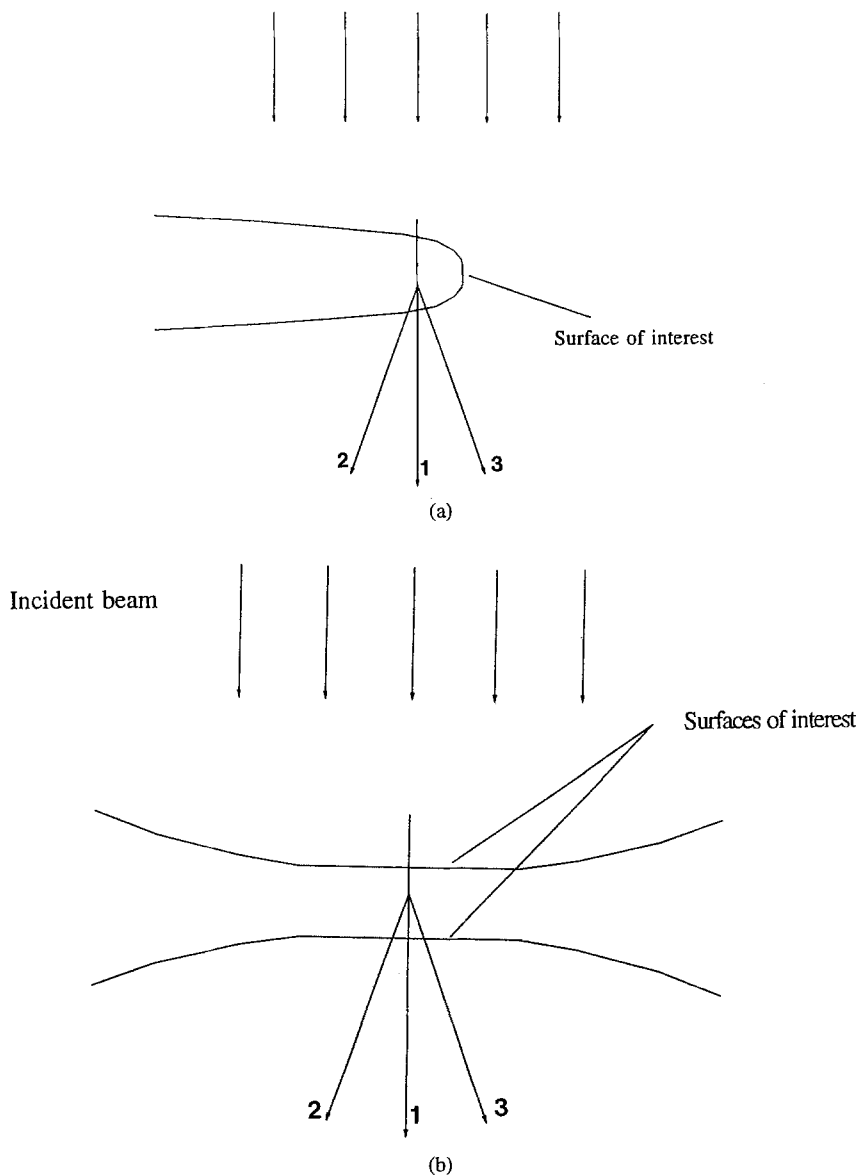
Fig. 2.   Electron beam geometry with respect to the specimen for the two imaging modes described in the text a) profile imaging and b) plan view imaging. In both cases, 1) represents the transmitted beam while 2) and 3) represent diffracted beams.

sublimation pumps (a combination of the latter two is used in [91]).

This alternative approach to designing an UHV-TEM-surface science facility i.e to eliminate the cryofinger on the column and in addition, adding the surface science accessories onto a separate UHV module has been adopted by our group. The microscope used in the studies here is a Hitachi 300 keV H9000 electron microscope which has been modified in the region of the objective (and above and below it also) so

that the operating pressure at the sample (i.e. the objective region) is 1×10^{-10} Torr. The pressure quoted above is stable for periods of a few months; the primary residual gas at the specimen is water vapor coming from below the specimen region where the pumping is conduction limited. Attached to the side of the microscope is a UHV-Surface Science Chamber (UHV-SSC); specimens are loaded into the transfer chamber via a loadlock mechanism. Both the microscope and the side chamber are pumped using a combination of

turbomolecular pumps, home-built titanium sublima-
tion pumps and ion pumps. A schematic of this setup
is shown in Fig. 3 and a more detailed review of this
instrument is provided in [78].

Specimen Preparation

Since the quality of the final information obtained is
influenced mainly by the sample preparation itself,
considerable time and effort are expended in prepar-
ing electron transparent specimens for conventional
HREM. Such *ex situ* (outside the UHV chambers)
preparation procedures usually involve some combi-
nation of mechanical polishing/lapping, dimpling and
finally ion-milling to create a hole at the center of
the specimen, thin electron transparent regions usually
abound around the hole. This stage is then followed by
further preparation under UHV conditions until clean
surfaces/interfaces can be obtained. In our case, the lat-
ter step is carried out inside the UHV-SSC and subjects
the pre-thinned sample to a combination of ion-beam
cleaning and annealing treatments (unique to each sam-
ple) until well-characterized, reproducible (to establish
any kind of database for meaningful scientific interpre-
tation) clean surfaces are obtained.

While the ion beam cleaning and annealing combina-
tion seems to work pretty effectively for most metal sys-
tems, the damage induced by the ion-milling technique
in some cases are very difficult, sometimes impossible,
to remove even after numerous high temperature an-
nealing cycles. For example, with noble metals i.e.
Au(001) [94–95] and Ag(110) [96], Xe ions used for
milling have extremely large penetration depths into the
material. These can be driven away only by subsequent
very high temperature anneal treatments which on the
other hand coarsens the sample. Such a coarsening
effect is not altogether undesirable since as analyzed
theoretically by Srolovitz [97], an instability develops
which leads to a thin region just behind a thicker outer
edge of the hole as illustrated in Fig. 4, ideal for fur-
ther study. The ion beam cleaning also fails in case of
some compound semiconductors e.g. GaAs (001) [98],
where argon ion milling at 3 kV preferentially sputters
the arsenic leaving gallium particles on the surface.
Our experience is that sample preparation, not the ex-
perimental electron microscopy, is the rate and science
limiting step.

To conclude this section, it is appropriate to make
a few comments which may highlight some of the pe-
culiarities of electron microscopy in UHV. One of the

earliest lessons for us was that absolute vacuum levels
are close to irrelevant; what is critical is the partial pres-
sures of the background gases during active processes,
e.g. thin film deposition, annealing and ion sputtering.
For instance, it was observed during work on Au [94]
when sputtering with Xe that unless the hydrocarbon
background was $<10^{-9}$ Torr with a Xe pressure of 10^{-6}
Torr, the surfaces were contaminated with carbon. Hy-
drocarbons are not the only problem molecules; we
found that CO desorption due to secondary electrons
reaching an evaporator filament suppressed the 5×1
surface reconstruction of Ir(001) [51]. Water vapor
(H_2O) on the other hand limited the lifetime of the
Si(100)-2 × 1 surface to the order of a few hours in-
side the microscope [99]. Since HREM's use electrons
generated at very high voltages, one should be aware
of the possibility of radiation damage, as is commonly
seen in case of transition metal oxides [95, 100–104].
Such damage processes can be important for a surface;
we have recently observed dereconstruction of the Au-
Si(111)-5 × 1 surface [105] by knockon damage with
a threshold of $\sim$250 kV.

Sample System Results

Due to the problems with clean surface preparation
as outlined in the previous sections, to the best of our
knowledge, studies by other UHV-TEM groups around
the world have been limited to surfaces of materials (ex-
cluding oxides) with low intrinsic sticking coefficients
such as gold [106–109], which can be prepared by
evaporation, and silicon which can be cleaned by self-
heating [76, 110–111] or gas reaction etching [112]. In
this section, we present results on the clean surfaces of
some metals and semiconductors that have been stud-
ied using UHV-HREM and diffraction mainly by our
group here at Northwestern University. For reasons of
brevity, the effect of the UHV environment on ceramic
oxide surfaces i.e. radiation damage and annealing
behavior etc. will not be discussed here and the inter-
ested reader is referred to the appropriate refs. CoO
[95], WO_3 [95, 100], ReO_3 [101], Al_2O_3 [102], NiO
[103], TiO_2 [104], V_2O_5 [95, 113–114].

Diffraction Contrast Imaging

En route to preparing a thin surface for HREM, the sam-
ple morphology undergoes numerous changes which
can be charted using a combination of bright field-
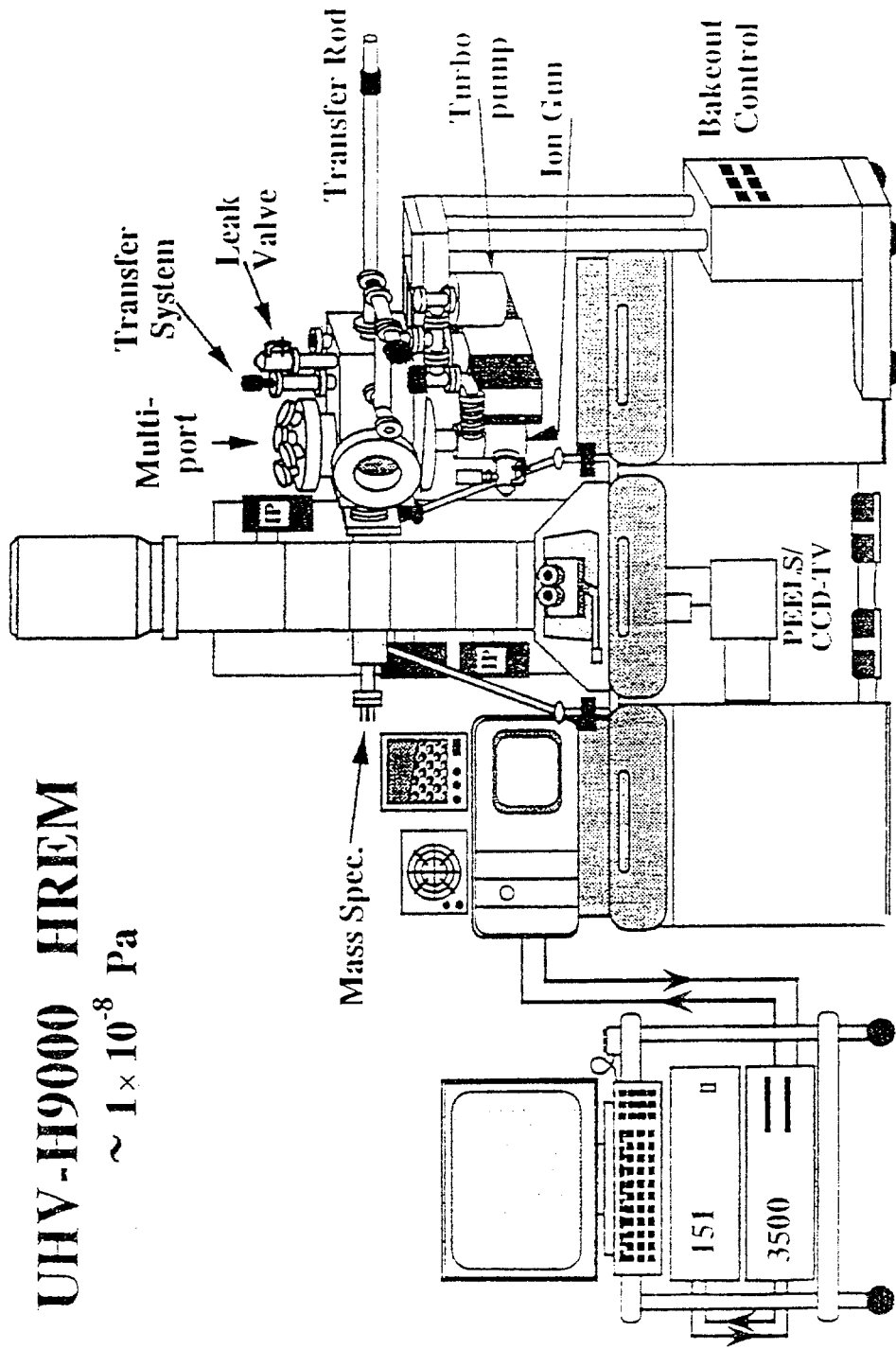dark field (BF-DF) imaging techniques. While surface

Fig. 3. A schematic diagram of the UHV-HREM facility at Northwestern University. Attached to the UHV-HREM column via a welded bellows is the UHV-SSC. Both the Gatan PEELS and the CCD-TV units are interfaced to an Apollo 3500 workstation, the latter via an Imaging Technology 151 framestore unit.
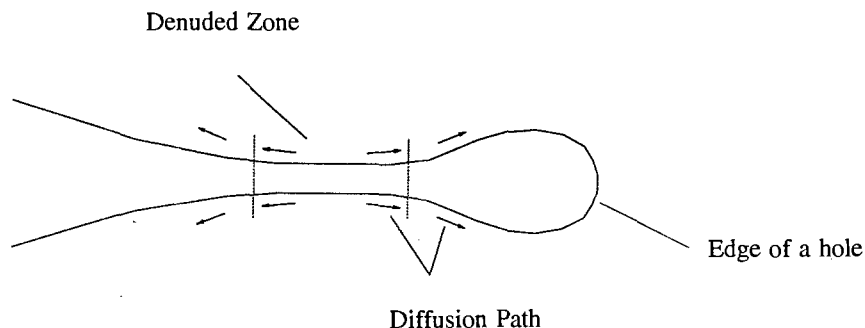
Denuded Zone

Edge of a hole

Diffusion Path

Fig. 4. Surface instability effect seen during coarsening results in a denuded zone/thin area, within the dotted lines, just inside the thicker outer edge. Arrows show the direction of atomic diffusion.

ordering is usually accompanied by a decrease in the defect density of the material and rounding off of the edges of the holes [51, 95, 103], there always exists a high density of subsurface defects ($\sim 10^{11}$–10^{13} cm^{-2}) in equilibrium with the clean reconstructed surfaces [49]. It has been noticed in these cases that while sharp spots are seen in the diffraction patterns, the accompanying BF-DF images reveal the presence of numerous impurity and/or defect clusters (1–10 nm in size) coexisting with the surface reconstruction. The actual nature of these vary from system to system e.g. while Fig. 1 clearly shows that in case of Si(111)-7 × 7, the reconstruction seems to co-exist with numerous stacking faults and stacking fault tetrahedra in the bulk of the material [49, 115], in case of Ir(001)-5 × 1, IrO$_2$ particles co-exist with the surface reconstruction as illustrated in Fig. 5. Other surface defects e.g. steps can also be imaged using these modes and in case of Ir(001) surface, the evolution of the steps as a function of annealing has been charted using the (1 × 1) reflections [51]. A common factor in all surface science studies using the UHV-HREM is that the (1 × 1) spots grow sharper and steps develop into wider terraces as a function of repeated annealing treatments.

Phase Contrast Imaging

High resolution imaging can be carried out in two modes i.e. conventional HREM, where the electron beam is parallel to one of the major zone axes or off-zone HREM where the crystal is tilted off to damp the strong Bragg beams. Examples of the Ir(001)-5 × 1 system are used to illustrate the different aspects of HREM imaging. Figure 6 shows an Ir(001)-5 × 1 surface imaged using the on-zone axis HREM mode. When looking at surface structures, the on-zone mode

of imaging is not particularly useful since it shows contribution mainly from the bulk diffraction spots and moire fringes due to the reconstructed surface. Also, the contrast levels of the surface structure are very low (5–6%) in the on-zone mode [116] and thus unless sufficient care is taken, surface information would be swamped away by the bulk lattice contrast. Higher sensitivity to the surface layer can be obtained by tilting the crystal off the zone (essentially damping out the bulk contrast) and an example of a HREM image taken off the zone is shown in Fig. 7. A region showing a hexagonal lattice is seen on one side of the image (this is interpreted as a region where the bulk stacking sequence is perfectly terminated while the surface structure showing a periodicity of "5" in one direction can be seen on the other side of the image. Surface steps can be seen in this image separating the two regions. In summary, information about the surface structure is more readily obtained when the crystal is tilted off the zone axis due to an increase in the intensities of the surface spots relative to the bulk.

Although HREM images reveal information about atom positions on the surface, these are not powerful enough in certain cases in resolving disputes between different models proposed for the surface when the absolute shift between the atom positions in the models are extremely small. Two such instances are for the Ir(001)-5 × 1 and the Si(001)-2 × 1 surfaces where the absolute shift between the atom positions for the two models proposed in the literature are 0.016 nm [117] and about 0.005 nm [118] respectively. In these cases, intensities from transmission diffraction patterns are analyzed in a manner similar to LEED and XRD investigations to yield information accurate at the necessary level. Examples of the two above mentioned surfaces will be detailed in the following section.
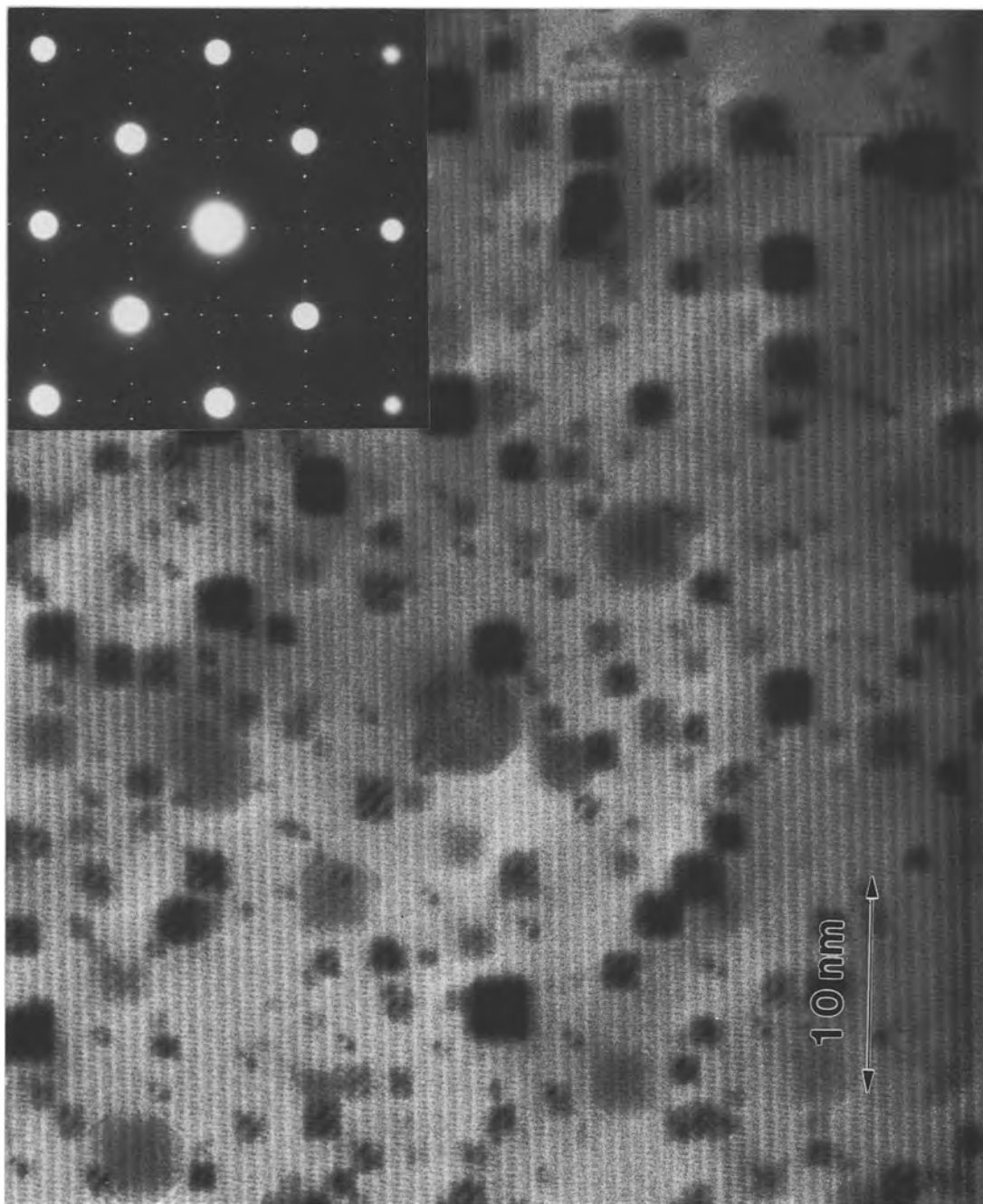
Fig. 5. Dark field image showing the moire fringes arising from the Ir(001)-5 × 1 reconstruction, the inset diffraction pattern clearly shows the two domains of the reconstruction. Clearly seen existing with the reconstruction are square shaped particles, identified as IrO_2.
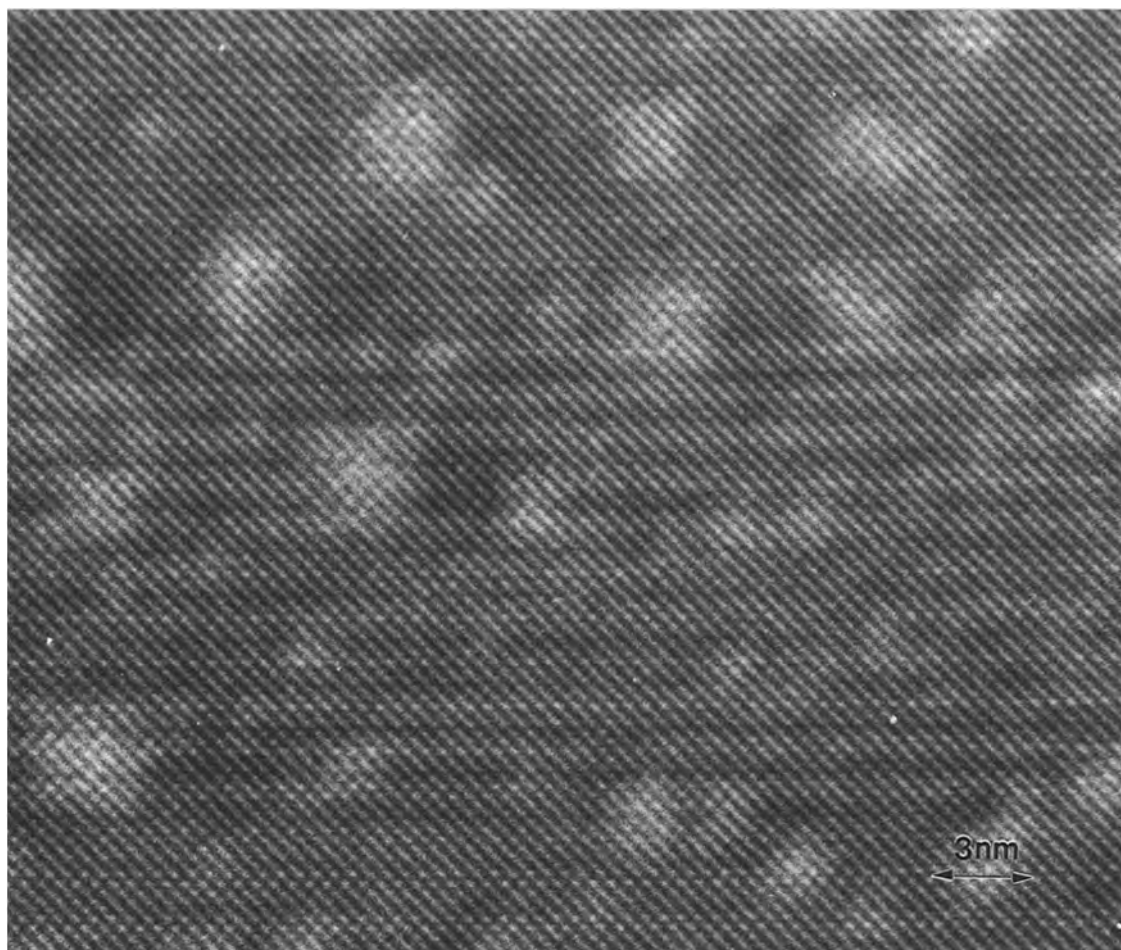
Fig. 6. An on-zone HREM image of the Ir(001)-5 × 1 surface showing moire fringes from the reconstruction. The surface contrast is swamped by the stronger bulk diffraction.

Diffraction

Long before the advent of imaging techniques to look at the fine atomic details of the surface, intensities in x-ray diffraction and LEED patterns were used for this purpose. For some excellent review articles on these techniques the reader is referred to XRD [8–9] and LEED [119–120] and the theory of the tests used in these techniques can be found in [121–122]. The field of electron diffraction intensity analysis to yield surface/interface structure information is in comparison a relatively new field and was used for the first time to solve the Si(111)-7 × 7 surface structure [73]. While the earlier TED studies used a kinematical intensity calculation approach [73, 111], because of its simplicity such an approach can be inadequate [123]. Rigorous full scale dynamical calculations have been shown to be power-

ful in determining the Ir(001)-5 × 1 [124] and Si(001)-2 × 1 surface structures [99] as will be demonstrated in the following sections. In this case, intensities are calculated for previously proposed structure models and the differences between the corresponding theoretical values and the experimentally observed intensities are sought to be minimized to yield the final structure.

Examples of the Ir(001)-5 × 1 and Si(001)-2 × 1 surfaces will be briefly discussed in this section to illustrate the potency of this technique in resolving surface structures. Conventionally, a series of diffraction patterns were recorded at different exposure times (for each tilt and thickness condition) to envelope the dynamic range of the intensities of the surface and bulk spots. Figures 8a and 8b show such patterns recorded for Ir(001)-5 × 1 and Si(001)-2 × 1 surfaces (for details on specimen preparation, refer to [51] and [99]
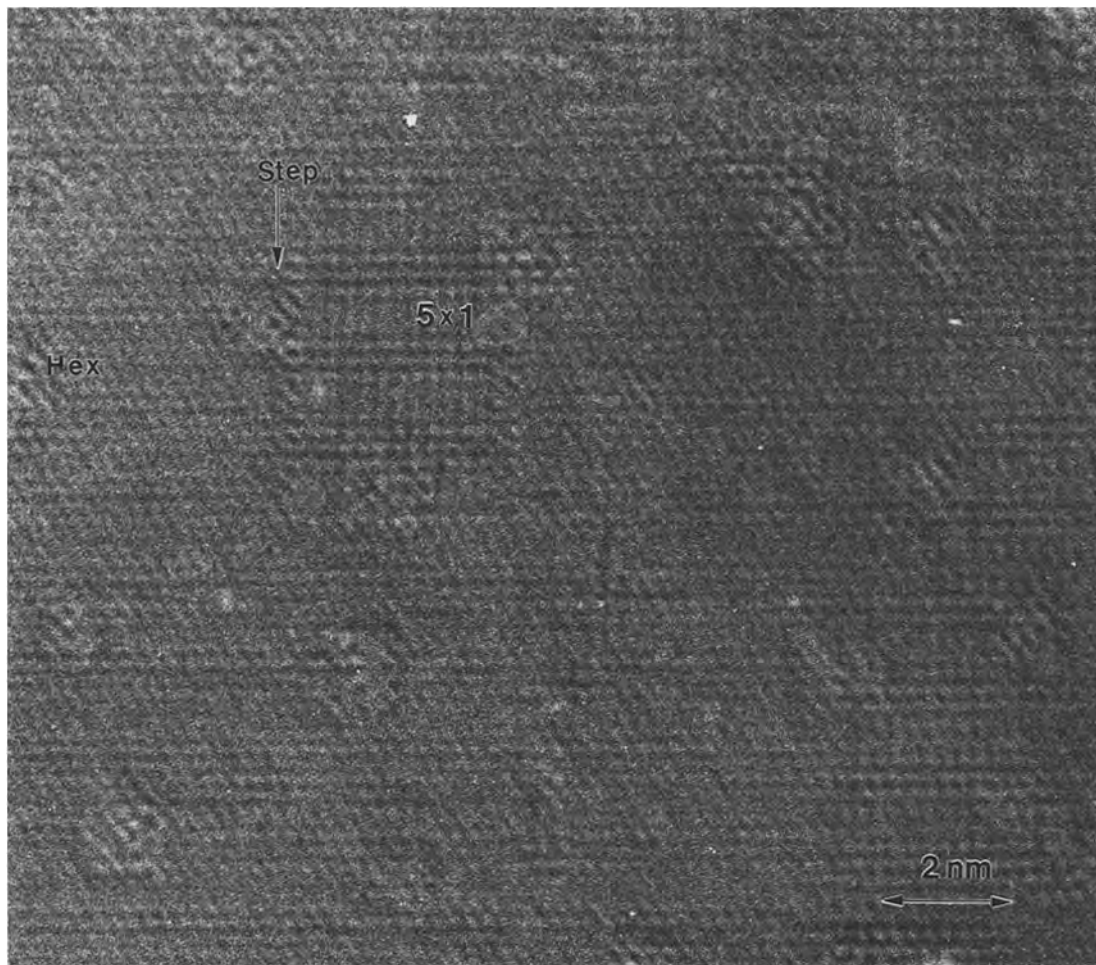
Fig. 7. An off-zone HREM image of the Ir(001)-5 × 1 surface showing a higher contrast from the surface structure. A surface step (arrowed) can be seen separating the regions with a 5 × 1 structure on one side and the bulk structure on the other.

respectively). In both cases, a few bulk and surface spots have been arrowed and characterized (in terms of the surface unit cell) to show the different domains of the reconstructions. The diffraction patterns were digitized to 8-bits using an Optronics P1000 microdensitometer (absolute value for some of the stronger spots were measured using PEELS [125]). The absolute intensity values were obtained by removing the background using a high pass filter and integrating the intensity around each spot in case of Ir and by using a cross-correlation technique in case of Si [126]. Two sets of data (from the two orthogonal domains in both systems) were obtained from each pattern; typically each data set had ~100–200 beams.

Dynamical diffraction intensities for the spots corresponding to the different structure models in the

literature (for the two systems) were then simulated for the known thickness and tilt conditions. The difference between the theoretical i.e. simulated and the experimental intensities for the surface spots were then calculated (R-factor) and the atomic positions for the model that would provide the minimum value of the R-factor yielded the optimized structure. However, the lowest value of the R-factor cannot be the sole factor determining the final structure, since systematic errors could lead to a local minimum rather than a global minimum i.e. the solution has to be physically realistic. In both the systems involved, this was found to be true when the surface layers were allowed to relax freely since low values for R-factors could be obtained for unphysical atom position solutions. On the other hand, when the solutions were constrained by imposing a well-defined
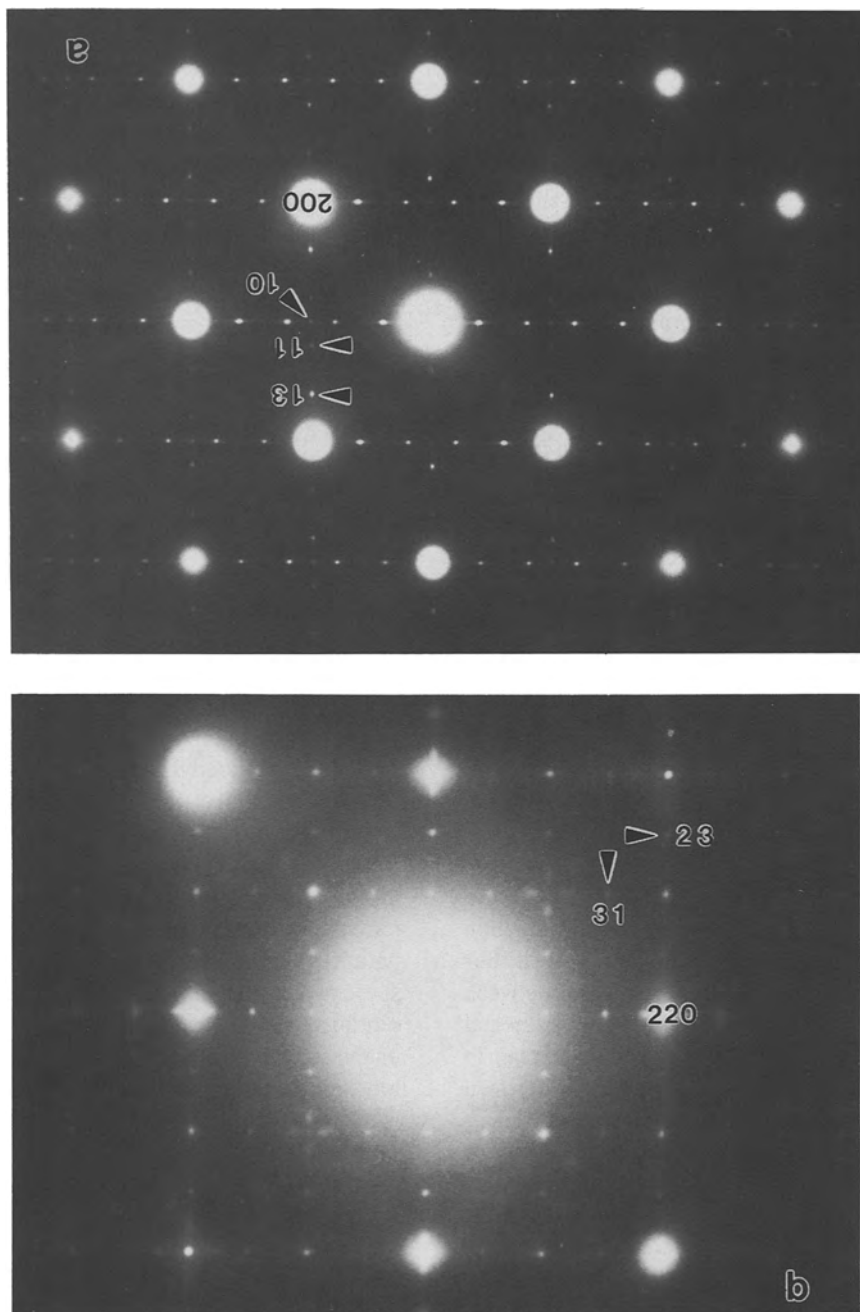
Fig. 8. Sample diffraction patterns taken from a) an Ir(001)-5 × 1 surface and b) a Si(001)-2 × 1 surface. The surface spots are indicated by arrows and a bulk spot is also indexed for reference.

long range strain field associated with surface relaxation, realistic atom positions were obtained at 90% confidence level albeit with slightly higher values for the R-factor. In case of Si(001), since the R-factors associated with the two competing structures differed only by 0.02, error analyses of the atom positions for the two structures were carried out (we had not attained this level of sophistication when analyzing the Ir data). Reduced χ^2 values of ~1–1.5 were obtained for one of the structures i.e. asymmetric dimer model

compared to values of 1.5–2.0 for the other i.e. symmetric model. Since the lower R-factor values were also associated with the asymmetric model, this structure was proposed for the surface.

Although this type of approach can be very powerful, a word of caution is appropriate. Although diffraction intensities via a Patterson function can suggest a model, e.g. for the Si(111)-7 × 7 surface [73] or refine the atomic positions within a structure, it cannot always solve an unknown surface structure. This is an example of the classic phase problem in diffraction where the Patterson function need not have a unique solution in terms of the atomic positions. We have recently encountered this with the Au-Si(111)-5 × n surface, where the electron diffraction Patterson function matches the x-ray diffraction Patterson function [127], but does not determine the structure. What is required is real space data to determine approximate atomic positions for further refinement, either from STM or HREM. It is relevant to note that for the silicon-gold system, STM has to date failed to determine atomic positions [128–130].

Discussion

The main focus of this note has been UHV electron microscopy of surfaces, with some inclusion of monolayer growth of metals on the surfaces of semiconductors. Whereas the solid-vacuum junction is an interface, solid-solid interfaces are slightly different and there may appear to be little correlation between the two. However, achieving controllable experimental data from clean surfaces is a critical intermediate step to controlled UHV electron microscopy of *in-situ* grown interfaces. The potential of this type of approach is quite substantial; of all the techniques discussed earlier that can obtain information about surfaces, only transmission electron microscopy and x-ray diffraction can be used for a buried interface. Given a good sample (not a trivial issue) all the transmission electron microscopy techniques described above to obtain information about a surface can be used essentially without change to look at a buried interface.

Ex situ cross-sectioning and plan-view imaging of (after air transfer) of UHV prepared samples has had spectacular success in finding several interface structures, but suffer from their inability to study the dynamics of the interface not to mention the ever present danger of sample preparation artifacts and sample contamination. We believe that analysis of samples grown

under UHV conditions within the microscope or in an attached surface science chamber is a new area which will see quite substantial growth in the near future; at the time of writing this paper we, and several other groups around the world are in the process of commissioning multichamber systems attached to UHV transmission electron microscopes.

Note Added in Proof

In the time elapsed between submission of the paper and its publication, our group has made significant advances in the fields of instrumentation and information retrieval from micrographs.

A multichamber Specimen-Preparation, Examination and Analytical Research (SPEAR) facility [131] has replaced the UHV-SSC shown in Fig. 3. It includes a Molecular Beam Epitaxy chamber for thin film growth, a central transfer chamber with metal evaporation filaments and an analytical module equipped with X-ray photoelectron spectroscopy, Auger electron spectroscopy and scanning electron microscopy capabilities. An imaging duoplasmatron ion gun is mounted on the analytical chamber to facilitate low energy, shallow angle surface cleaning while specimen annealing is done resistively.

Substantial advances have also been made in understanding surface structures using HREM and quantitative electron diffraction. The atomic structures of the Au-Si(111)-$\sqrt{3} \times \sqrt{3}$ [132] and Au-Si(111)-5×2 [133] surfaces have been determined in great detail. In the former case, Au and Si atoms in Au-Si(111)-$\sqrt{3} \times \sqrt{3}$ form trimers which twist by a few degrees about their centers. Also from the HREM data, the surface domain walls were found to be vacancy type or the Au to Au spacing was near the Si(1 × 1) type spacing, an important fact considering the small surface domains of this structure (5 nm). Au atoms in the Au-Si(100)-5 × n system [134] have also been located exclusively using a phase retrieval procedure from HREM images (used also in the analysis of the Au-Si(111)-5 × 2 system).

A qualitative analysis of HREM images from the Ag-Si(100)-2 × 1 system [135] was used on the other hand to explain for the first time, the morphology of three-dimensional islands of Ag that nucleate on Si(100)-2 × 1 surfaces at room temperature. It was shown that contrary to the existing belief in the literature about simple single crystal structures for the Ag islands, their morphology actually comprises of a mixture of single crystal and multiply twinned structures. This study also underlined the need for strict control over vacuum conditions since changes in morphology were observed on exposure to air.

References

1. J.A. Venables, G.D.T. Spiller, and M. Hanbücken, Rep. Prog. Phys. **47**, 399 (1984).
2. R. Kern, G. LeLay, and J.J. Métois, in *Current Topics in Materials Science*, Vol. 3, edited by E. Kaldis (North-Holland Publishing Company, 1979), p. 135.
3. J.A. Venables, Ultramicroscopy **7**, 81 (1981).
4. J.A. Venables, D.R. Batchelor, M. Hanbücken, C.J. Harland, and G.W. Jones, Phil. Trans. Roy. Soc. A **318**, 243 (1986).
5. J.M. Cowley, Am. Chem. Soc. Symp. Ser. **248**, 353 (1985).
6. J.M. Cowley, in *Mat. Res. Soc. Symp. Proc.* 31, edited by W. Krakow, D.A. Smith, and L.W. Hobbs (Elsevier Science Publishing Company, New York, 1984), p. 177.
7. D.J. Smith, J. Vacuum Sci. Technol. B **3**, 1563 (1985).
8. I.K. Robinson and D.J. Tweet, Rep. Prog. Phys. **55**, 599 (1992).
9. R. Feidenhans'l, Surf. Sci. Rep. **10**, 105 (1989).
10. N. Osakabe, Y. Tanashiro, and K. Yagi, Surf. Sci. **109**, 353 (1981).
11. K. Yagi, A. Yamanaka, and H. Yamaguchi, Surf. Sci. **283**, 300 (1993).
12. H. Yamaguchi, Y. Tanashiro, and K. Yagi, Appl. Surf. Sci. **60/61**, 79 (1992).
13. C. Alfonso, J.M. Bermond, J.C. Heyraud, and J.J. Métois, Surf. Sci. **262**, 371 (1992).
14. Y. Ma, S. Lordi, P.K. Larsen, and J.A. Eades, Surf. Sci. **289**, 47 (1993).
15. P.K. Larsen and G. Meyer-Ehmsen, Surf. Sci. **240**, 168 (1990).
16. B. Bolger and P.K. Larsen, Rev. Sci. Instrum. **57**, 1363 (1986).
17. W. Telieps and E. Bauer, Surf. Sci. **162**, 163 (1985).
18. M. Mundschau, E. Bauer, W. Telieps, and W. Swiech, Surf. Sci. **223**, 413 (1989).
19. R.M. Tromp and M.C. Reuter, Phys. Rev. Lett. **68**, 820 (1992).
20. R.J. Phaneuf, N.C. Bartelt, E.D. Williams, W. Swiech, and E. Bauer, Phys. Rev. Lett. **21**, 2986 (1991).
21. M. Mundschau, E. Bauer, W. Telieps, and W. Swiech, Surf. Sci. **213**, 381 (1989).
22. M. Mundschau, E. Bauer, W. Telieps, and W. Swiech, J. Appl. Phys. **65**, 4747 (1989).
23. M. Mundschau, E. Bauer, and W. Swiech, J. Appl. Phys. **65**, 581 (1989).
24. J. Tersoff, A.W. Denier van der Gon, and R.M. Tromp, Phys. Rev. Lett. **70**, 1143 (1993).
25. R.E. Schlier and H.E. Farnsworth, J. Chem. Phys. **30**, 917 (1959).
26. S.Y. Tong and A.L. Maldonado, Surf. Sci. **78**, 459 (1978).
27. L.H. Veneklasen, Rev. Sci. Instrum. **63**, 5513 (1992).
28. M.S. Altman, H. Pinkvos, J. Hurst, H. Poppa, G. Marx, and E. Bauer, in *Mat. Res. Soc. Symp. Proc.* Vol. 232, edited by Y. Sugita, B.M. Clemens, D.E. Laughlin, K. Ouchi, and T. Suzuki (North-Holland Publishing Company, New York, 1991), p. 125.
29. G. Ertl, Science **254**, 1750 (1991).
30. E. Bauer, M. Mundschau, W. Swiech, and W. Telieps, Ultramicroscopy **31**, 49 (1989).
31. W. Engel, M.E. Kordesch, H.H. Rotermund, S. Kubala, and A.V. Oertzen, Ultramicroscopy **36**, 164 (1991).
32. O.H. Griffith and G.F. Rempfer, Adv. in Optical and Elect. Microsc. **10**, 270 (1987).
33. H. Sato, Y. Tanashiro, and K. Yagi, Appl. Surf. Sci. **60/61**, 367 (1992).
34. B.P. Tonner, Nucl. Inst. and Meth. A **291**, 60 (1991).
35. G. Rempfer and M.S. Mauck, Optik **92**, 3 (1992).
36. J.A. Venables, D.J. Smith, and J.M. Cowley, Surf. Sci. **181**, 235 (1987).
37. G.W. Jones and J.A. Venables, Ultramicroscopy **18**, 439 (1985).
38. M. Futamoto, M. Hanbücken, C.J. Harland, G.W. Jones, and J.A. Venables, Surf. Sci. **150**, 430 (1985).
39. C.J. Harland and J.A. Venables, Ultramicroscopy **17**, 17 (1985).
40. G.G. Hembree and J.A. Venables, Ultramicroscopy **47**, 109 (1992).
41. J. Drucker, M. Krishnamurthy, and G. Hembree, Ultramicroscopy **35**, 323 (1991).
42. J. Drucker and M.R. Scheinfein, Phys. Rev. B **47**, 4068 (1993).
43. J. Liu and J. Cowley, Ultramicroscopy **48**, 381 (1993).
44. R.M. Feenstra and M.A. Lutz, Surf. Sci. **243**, 151 (1991).
45. M. Giesen, J. Frohn, M. Poensgen, J.F. Wolf, and H. Ibach, J. Vac. Sci. Tech. A **10**, 2597 (1992).
46. N. Kitamura and M.B. Webb, Bull. Am. Phys. Soc. **38**, 509 (1993).
47. M.G. Lagally, Y.W. Mo, R. Kariotis, B.S. Swartzentruber, and M.B. Webb, in *Kinetics of Ordering and Growth at Surfaces*, edited by M.G. Lagally (Plenum Press, New York, 1990).
48. P.A. Bennett, M. Copel, D. Cahill, J. Falta, and R.M. Tromp, Phys. Rev. Lett. **69**, 1224 (1992).
49. D.N. Dunn, P. Xu, and L.D. Marks, J. Cryst. Growth **125**, 543 (1992).
50. Y. Hana and K. Takayanagi, Ultramicroscopy **45**, 95 (1992).
51. D.N. Dunn, P. Xu, and L.D. Marks, Surf. Sci. **294**, 308 (1993).
52. F.M. Ross and J.M. Gibson, Phys. Rev. Lett. **68**, 1782 (1992).
53. K. Yagi, A. Yamana, H. Sato, M. Shima, H. Ohse, S. Ozawa, and Y. Tanashiro, Prog. Theor. Phys. Suppl. **106**, 303 (1991).
54. G. Honjo, K. Takayanagi, K. Kobayashi, and K. Yagi, J. Cryst. Growth **42**, 98 (1977).
55. L.D. Marks, in *Topics in Current Physics*, edited by W. Schommers and P. von Blanckenhagen, Vol. 71 (Springer-Verlag, Berlin, 1986), p. 71.
56. D.J. Smith, in *Chemistry and Physics of Solid Surfaces VI*, edited by R. Vanselow and R. Howe (Springer-Verlag, Berlin, 1986), Chapter 15.
57. J.M. Cowley, J. Vac. Sci. Tech. A **7**, 2823 (1989).
58. J.M. Cowley, Prog. Surf. Sci. **21**, 209 (1986).
59. L.D. Marks, Surf. Sci. **139**, 281 (1984).
60. L.D. Marks, Phys. Rev. Lett. **51**, 1000 (1983).
61. L.D. Marks and D.J. Smith, Nature **303**, 316 (1983).

62. N. Ikarashi, K. Kobayashi, H. Hoike, H. Hasegawa, and K. Yagi, Ultramicroscopy **26**, 195 (1988).

63. J.M. Gibson, M.L. McDonald, and F.C. Unterwald, Phys. Rev. Lett. **55**, 1765 (1985).

64. M. Mitome and K. Takayanagi, Surf Sci. **242**, 69 (1991).

65. P. Lu and D.J. Smith, Phys. Rev. Lett. **59**, 2177 (1987).

66. D. Cherns, Phil. Mag. **30**, 549 (1974).

67. G. Lempful and Y. Uchida, Ultramicroscopy **4**, 275 (1979).

68. S. Iijima, Ultramicroscopy **6**, 41 (1981).

69. W. Krakow and D.G. Ast, Surf. Sci. **58**, 485 (1976).

70. K. Kambe and G. Lehmpfuhl, Optik **42**, 187 (1975).

71. A.F. Moodie and C.E. Warble, Phil. Mag. **16**, 891 (1967).

72. K. Takayanagi, Y. Tanashiro, M. Takahashi, and S. Takahashi, J. Vac. Sci. Tech. A **3**, 1502 (1985).

73. K. Takayanagi, Y. Tanashiro, S. Takahashi, and M. Takahashi, Surf. Sci. **164**, 367 (1985).

74. Z. Lilienthal-Weber, R. Gronsky, J. Washburn, N. Newman, W.E. Spicer, and E.R. Weber, J. Vac. Sci. Tech. B **4**, 912 (1986).

75. K. Takayanagi, Y. Tanashiro, K. Kobayashi, K. Akiyama, and K. Yagi, Jap. J. App. Phys. **26**, L957 (1987).

76. K. Takayanagi, Y. Tanashiro, T. Ishitsuka, and K. Akiyama, App. Surf. Sci. **41**, 337 (1989).

77. F.K. LeGoues, M. Liehr, M. Riener, and W. Krakow, Phil. Mag. B **57**, 179 (1988).

78. J.E. Bonevich and L.D. Marks, Microscopy **22**, 95 (1992).

79. T.A. McLauchlan, R.S. Sennett, and D.G. Scott, Can. J. Res. **28** A, 530 (1950).

80. G.A. Bassett, in *Proc. Intern. Symp. on Condensation and Evaporation of Solids*, edited by E. Rutner, P. Goldfinger, and J.P. Hirth (Gordon and Breach, New York, 1962), p. 599.

81. A.E. Ennos, Br. J. App. Phys. **4**, 101 (1953).

82. H. Poppa, J. Vac. Sci. Technol. **2**, 42 (1965).

83. A. Barna, P.B. Barna, and J.F. Pocza, Vacuum **17**, 2 (1967).

84. R.J. Wilson and P.M. Petroff, Rev. Sci. Instrum. **54**, 1534 (1983).

85. R.D. Moorhead and H. Poppa, in *Proc. of the 27th Annual EMSA Meeting*, edited by C.J. Arceneaux (San Francisco Press, Inc., San Francisco, 1969), p. 116.

86. U. Valdré, E.A. Robinson, D.W. Pashley, M.J. Stowell, and T.J. Law, J. Phys. E **3**, 501 (1970).

87. K. Takayanagi, K. Yagi, K. Kobayashi, and G. Honjo, J. Phys. E **11**, 441 (1978).

88. H. Poppa, in *Epitaxial Growth*, edited by J.W. Matthews (Academic Press, New York, 1975), p. 215.

89. J.J. Métois, S. Nitsche, and J.C. Heyraud, Ultramicroscopy **27**, 349 (1989).

90. M.L. McDonald, J.M. Gibson, and F.C. Unterwald, Rev. Sci. Instrum. **60**, 700 (1989).

91. M.T. Marshall, X. Tong, and J.M. Gibson, in *Proc. of the 51st Annual Meeting of EMSA*, edited by G.W. Bailey and C.L. Rieder (San Francisco Press, Inc., San Francisco, 1993), p. 640.

92. H. Poppa, K. Heinemann, and A.G. Elliot, J. Vac. Sci. Technol. **8**, 471 (1971).

93. D.J. Smith, M. Gajdardziska-Josifovska, P. Lu, M.R. McCartney, J. Podbrdsky, P.R. Swann, and J.S. Jones, Ultramicroscopy **49**, 26 (1993).

94. D.N. Dunn, R. Ai, T.S. Savage, J.P. Zhang, and L.D. Marks, Ultramicroscopy **38**, 333 (1991).

95. L.D. Marks, R. Ai, J.E. Bonevich, M.I. Buckett, D.N. Dunn, J.P. Zhang, M. Jacoby, and P. Stair, Ultramicroscopy **37**, 90(1991).

96. G. Jayaram and L.D. Marks, in *Proc. of the Air Force Workshop on Surface Reactions on Space Environment*, 1992.

97. D.G. Srolovitz and S.A. Safran, J. Appl. Phys. **60**, 255 (1986).

98. G. Jayaram and L.D. Marks, (unpublished).

99. G. Jayaram, P. Xu, and L.D. Marks, Phys. Rev. Lett. **71**, 3489 (1993).

100. S.R. Singh, H.J. Fan, and L.D. Marks, in *Proc. of the 47th annual meeting of EMSA*, edited by G.W. Bailey and E.L. Hall (San Francisco Press, Inc., San Francisco, 1989), p. 632.

101. R. Ai, H.J. Fan, and L.D. Marks, in *Proc. of the 49th annual meeting of EMSA*, edited by G.W. Bailey (San Francisco Press, Inc., San Francisco, 1991), p. 636.

102. J.E. Bonevich and L.D. Marks, Ultramicroscopy **35**, 161 (1991).

103. R. Ai, M.I. Buckett, D.N. Dunn, T.S. Savage, J.P. Zhang, and L.D. Marks, Ultramicroscopy **39**, 387 (1991).

104. M.R. McCartney and D.J. Smith, Surf. Sci. **250**, 169 (1991).

105. R. Plass, G. Jayaram, and L.D. Marks, in preparation.

106. N.D.S. Canning, D. Outka, and R.J. Madix, Surf. Sci. **141**, 240 (1984).

107. D.A. Outka and R.J. Madix, Surf. Sci. **179**, 347 (1987).

108. K. Yagi, K. Takayanagi, K. Kobayashi, N. Osakabe, Y. Tanashiro, and G. Honjo, Surf. Sci. **86**, 174 (1979).

109. K. Takayanagi, Ultramicroscopy **8**, 145 (1982).

110. D.H. Zehner and C.W. White, in *Laser Annealing of Semiconductors*, edited by J.M. Poate and J.W. Mayer (Academic Press, New York, 1982), p. 287.

111. J.M. Gibson, Surf. Sci. Lett. **239**, L531 (1990).

112. S. Ozawa, A. Yamanaka, K. Kobayashi, Y. Tanashiro, and K. Yagi, Jap. J. App. Phys. **29**, L655 (1990).

113. R. Ai, H.J. Fan, and L.D. Marks, Surf. Sci. **280**, 369 (1993).

114. L.D. Marks, V.A. Volpert, and R. Ai, Surf. Sci. **280**, 375 (1993).

115. D.N. Dunn, R. Ai, T.S. Savage, L.D. Marks, and K. Merkle, in *Proc. of the 49th annual meeting of EMSA*, edited by G.W. Bailey (San Francisco Press, Inc., San Francisco, 1991), p. 620.

116. L.D. Marks, P. Xu, D.N. Dunn, and J.P. Zhang, EMSA Bulletin **22**(3), 65 (1992).

117. M.A. Van Hove, R.J. Koestner, P.C. Stair, J.P. Biberian, L.L. Kesmodel, I. Bartos, and G.A. Somorjai, Surf. Sci. **103**, 189, 218 (1991).

118. N. Roberts and R.J. Needs, Surf. Sci. **236**, 112 (1990).

119. E. Zanazzi and F. Jona, Surf. Sci. **62**, 61 (1977).

120. P.M. Marcus and F. Jona, Appl. of Surf. Sci. **11/12**, 20 (1982).

121. W.C. Hamilton, Acta Cryst. **18**, 502 (1965).

122. G.B. Carpenter, in *Principles of Crystal Structure Determination*, (W.A. Benjamin Inc., New York, 1969), p. 196.

123. L.D. Marks, Ultramicroscopy **45**, 145 (1992).

124. L.D. Marks, P. Xu, and D.N. Dunn, Surf. Sci. **294**, 322 (1993).

125. P. Xu and L.D. Marks, Ultramicroscopy **45**, 155 (1992).

126. P. Xu, G. Jayaram, and L.D. Marks, Ultramicroscopy, **53**, 15 (1994).

127. Ch. Schamper, W. Moritz, H. Schulz, R. Feidenhans'l, M. Nielsen, F. Grey, and R.L. Johnson, Phys. Rev. B **43**, 12130 (1991).

128. J.D. Omahony, C.H. Patterson, J.F. McGilp, F.M. Leibsle, P. Weightman, and C.F.J. Flipse, Surf. Sci. Lett. **277**, L57 (1992).

129. A.A. Baski, J. Nogami, and C.F. Quate, Phys. Rev. B **41**, 10247 (1990).

130. T. Hasegawa, K. Takata, S. Hosaka, and S. Hosoki, J. Vac. Sci and Tech. A **8**, 241 (1990).

131. E. Landree, C. Collazo-Davila, D. Grozea, R. Plass, G. Jayaram, L.D. Marks, and P.C. Stair, in *Proc. of the 53rd Annual Meeting of MSA* (submitted).

132. R. Plass and L.D. Marks, Surf. Sci. (submitted).

133. L.D. Marks and R. Plass, (in preparation).

134. G. Jayaram and L.D. Marks, (in preparation).

135. N. Doraiswamy, G. Jayaram, and L.D. Marks, Phys. Rev. B (in press).